nature

https://doi.org/10.1038/s41586-019-1695-0

Supplementary information

Superconductors, orbital magnets and correlated states in magic-angle bilayer graphene

In the format provided by the authors and unedited

Xiaobo Lu, Petr Stepanov, Wei Yang, Ming Xie, Mohammed Ali Aamir, Ipsita Das, Carles Urgell, Kenji Watanabe, Takashi Taniguchi, Guangyu Zhang, Adrian Bachtold, Allan H. MacDonald & Dmitri K. Efetov

Supplementary Information

Superconductors, Orbital Magnets, and Correlated States in Magic Angle Bilayer Graphene

Xiaobo Lu[1], Petr Stepanov[1], Wei Yang[1], Ming Xie[2], Mohammed Ali Aamir[1], Ipsita Das[1], Carles Urgell[1], Kenji Watanabe[3], Takashi Taniguchi[3], Guangyu Zhang[4], Adrian Bachtold[1], Allan H. MacDonald[2] and Dmitri K. Efetov[1]*

1. ICFO - Institut de Ciencies Fotoniques, The Barcelona Institute of Science and Technology, Castelldefels, Barcelona, 08860, Spain
2. Department of Physics, University of Texas at Austin, Austin TX 78712, USA
3. National Institute for Materials Science, 1-1 Namiki, Tsukuba, 305-0044, Japan
4. Beijing National Laboratory for Condensed Matter Physics and Institute of Physics, Chinese Academy of Sciences, Beijing, 100190, China

*E-mail: dmitri.efetov@icfo.eu

CONTENTS

A. High Temperature Data

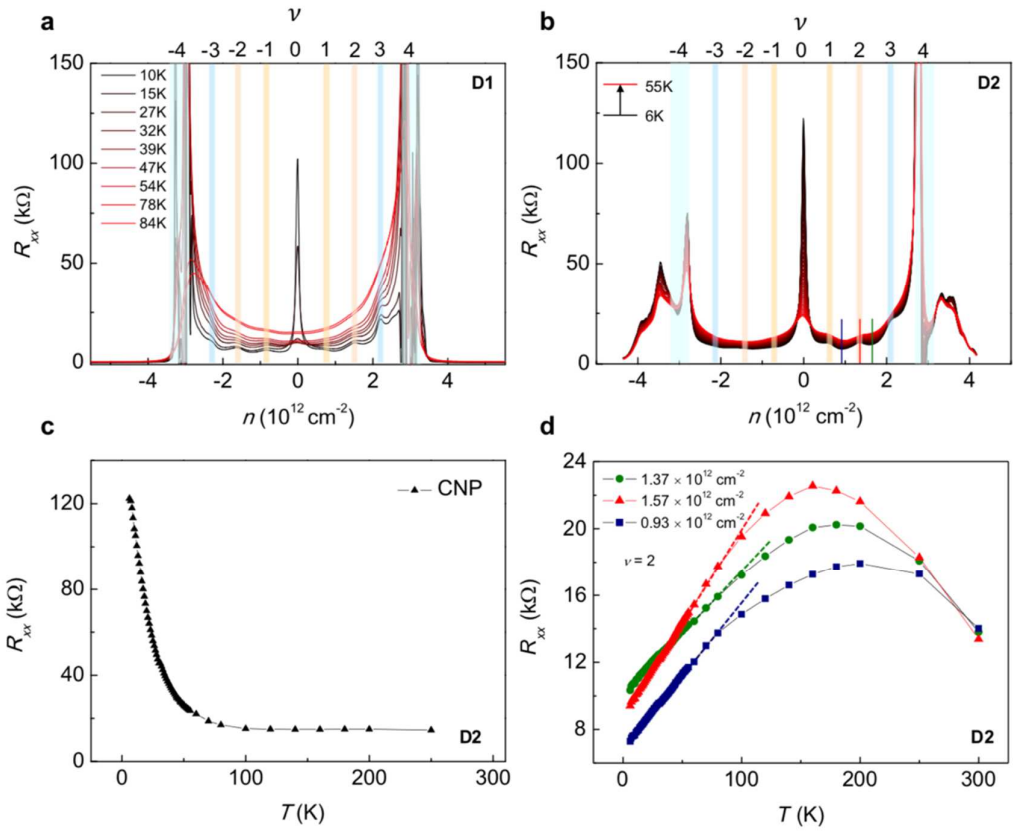

Figure S1 | High temperature transport measurements for Devices D1 and D2. a-b, R_{xx} vs. n for samples D1 and D2, respectively. **c,** CNP thermal activation behavior for device D2. **d**, R_{xx} vs. n line cuts for device D2 at charge carrier densities taken along lines indicated in b (color-coded).

For the general purpose of characterization Fig. S1 demonstrates R_{xx} vs. n scans taken at high temperatures for both samples D1 and D2. We observe the emergence of CNP at ~30 K for sample D1 and at ~90 K for sample D2. We also observe the appearance of local resistance maxima at the integer fillings of the superlattice unit cell for both samples at ~50 K. Fig. S1c shows thermal activation behavior for CNP of sample D2 from 6 K up to 250 K. Fig. S1d shows metal-like temperature dependencies for device D2 at the fillings shown on the Fig. S1b. Dashed lines demonstrate regions with the close-to-linear behavior.

B. Alignment Between Graphene and hBN in Device D1

Here we check the alignment between graphene and hBN in device D1. We extract the twist angle between graphene and top hBN $\approx 23\ (\pm 1.1)^{\circ}$ or $\approx 7\ (\pm 1.1)^{\circ}$, and between graphene and bottom hBN is $\approx 20\ (\pm 1.1)^{\circ}$ or $\approx 10\ (\pm 1.1)^{\circ}$. The uncertainty is ascribed to chirality of the edges in both graphene and hBN flakes.

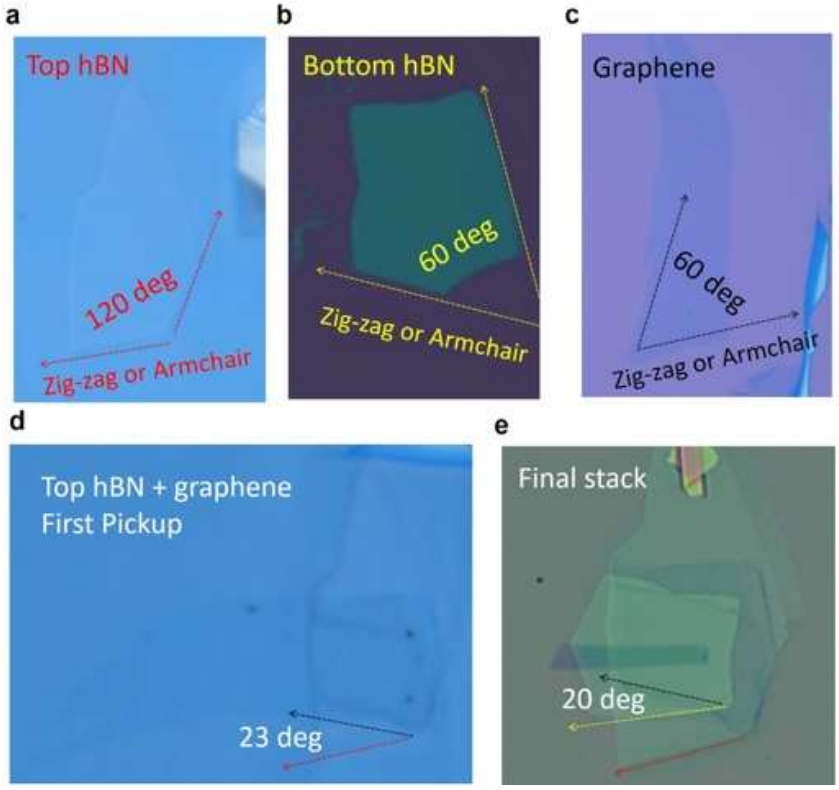

Figure S2 | Alignment between graphene and hBN. a, Optical image of top hBN flake on PC/PDMS stamp. **b,** Bottom hBN flake on SiO_2/Si substrate. **c**, Graphene flake on SiO2/Si substrate. **d**, Optical image showing the first pickup of graphene with top hBN. The twist angle between graphene and hBN is ~ 23 (± 1.1)° or 7 (± 1.1)°. **e**, Optical image if the final stack, showing the twist angle between bottom hBN and graphene is ~ 20 (±1.1)° or 10 (±1.1)°.

C. New Superconducting Domes Compared with Previous Works

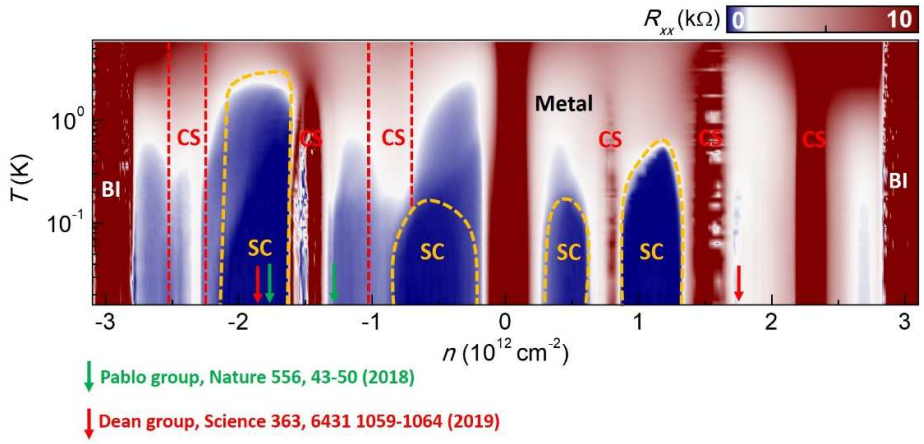

D. Signature of Fraunhofer Interference Patterns

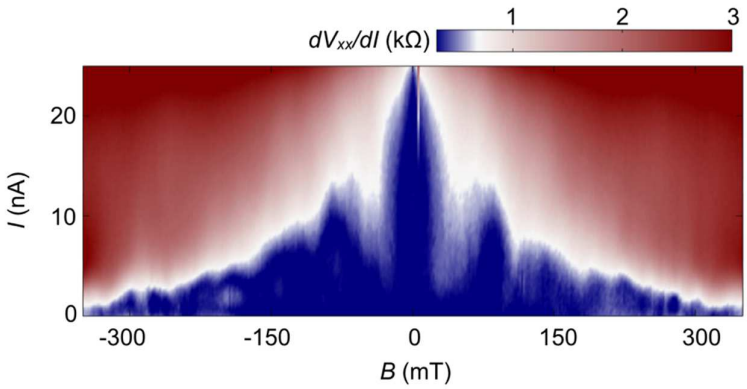

Figure S3 | Fraunhofer interference patterns measured at SC state with a carrier density of $1.11 \times 10^{12} cm^{-2}$.

E. Magnetic Field Effect on SC States

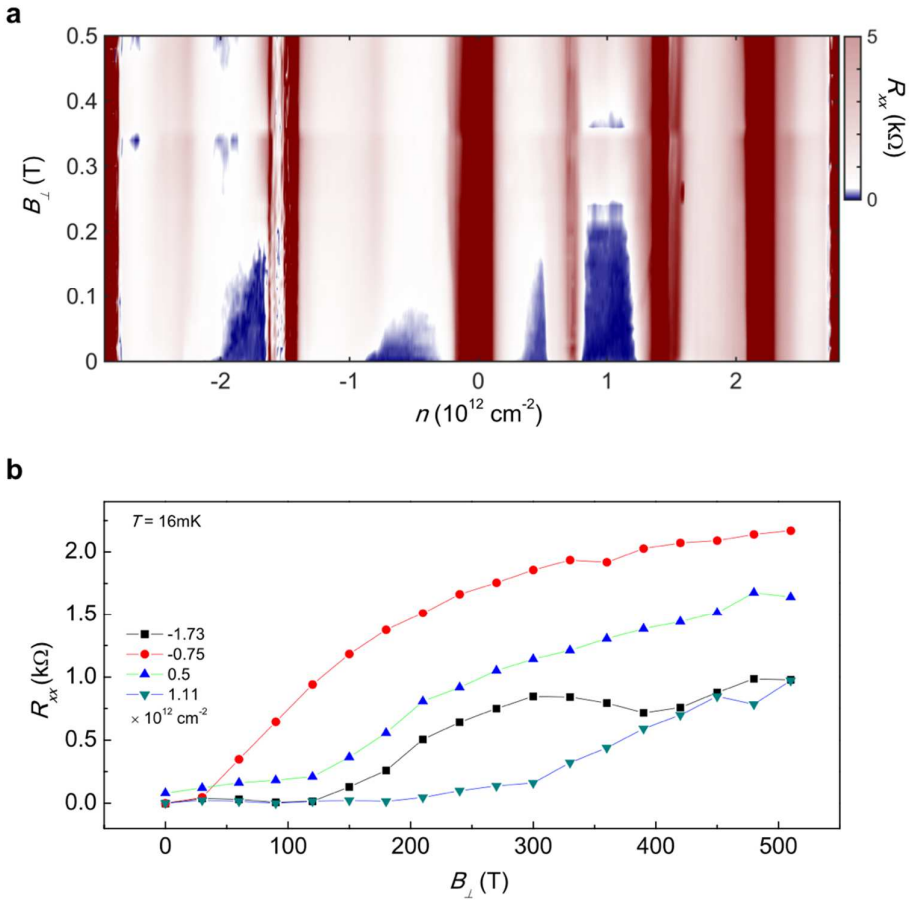

Figure S4 | Magnetic field measurement at base temperature. a, 2D map R_{xx} vs. $B\perp$, n. The blue regions indicated SCs. **b,** Line cuts R_{xx} vs. $B\perp$ for each of the SC pockets.

Fig. S4 demonstrates the effect of perpendicular magnetic field $B\perp$ on the SC pockets observed in sample D1. Fig. S4a shows 2D map of longitudinal resistance R_{xx} as a function of $B\perp$ and total charge carrier density n taken at the base temperature 16 mK. Fig. S4b shows R_{xx} vs. $B\perp$ taken at 16 mK for each SC at the optimal doping level

F. Zoomed-in Data for Phase Diagram Around $\nu = -1$, CNP and $\nu = 1$

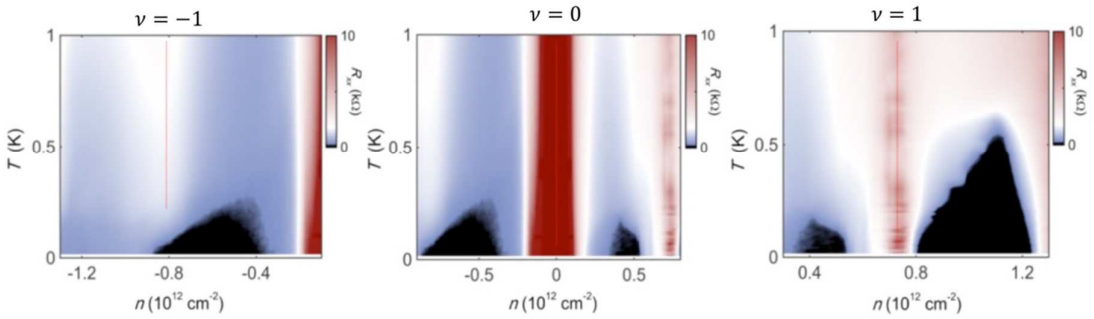

Figure S5 | Zoomed-in images of superconductor correlated insulator phases reported in Fig.1e in the main text. Black regions indicate resistance below 100 Ω. Red dashed lines indicate correlated gapped states. SC-CS phase diagram observed close to **a,** $\nu = -1$. **b,** CNP and **c,** $\nu = 1$.

G. Quantum Oscillations at High Densities

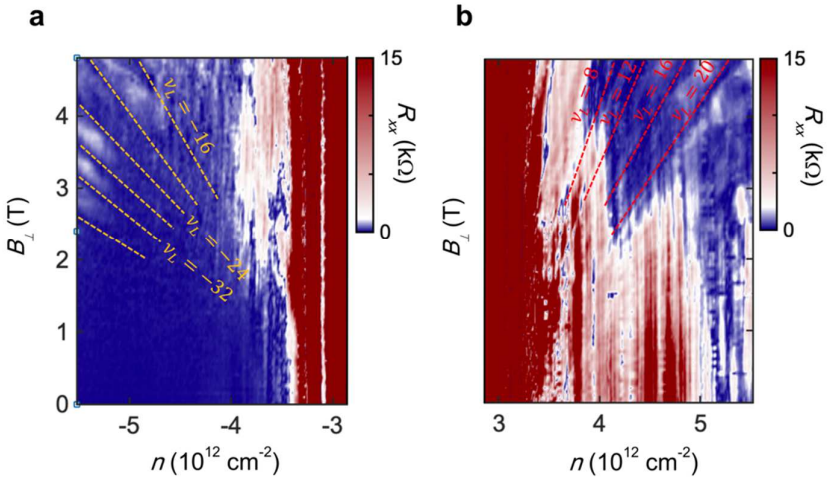

Figure S6 | SdH oscillation at high magnetic fields and high charge carrier densities beyond the band edges. SdH oscillations for electron (hole) sides are shown on **a (b).**

Fig. S6 a-b show R_{xx} vs. $B\perp$ and n taken at high charge carrier densities and high magnetic fields. The figure shows SdH quantum oscillations that appear outside the full-filled Moiré superlattice unit cell. We note that at high charge carrier densities the LL fan diagram follows that of Bernal stacked bilayer graphene. We observe a sequence of resistance dips corresponding to hole-like LL with integer fillings ν_L = 16, 20, 24, 28, 32, 36 (Fig. S6a) and electron-like LL with integer fillings ν_L = 8, 12, 16, 20 (Fig. S6b).

H. Quasiparticle Bandstructures of Insulating Ground States at $\nu = 0$

We performed self-consistent mean field calculations, adding to the Coulomb interactions starting from the non-interacting continuum model for twisted bilayer graphene[1]. Details of the calculation can be found in previous work[2]. One important parameter in our calculation is the ratio of intra-sublattice to inter-sublattice tunneling amplitudes T_{AA}/T_{AB} which controls the bandgap between flat bands and higher energy bands. Its value can be adjusted to account reasonably accurately for corrugation and lattice relaxation effects, which may be somewhat sample dependent. We use $T_{AA}/T_{AB} = 0.8$, appealing to the thorough previous DFT modelling study[3].

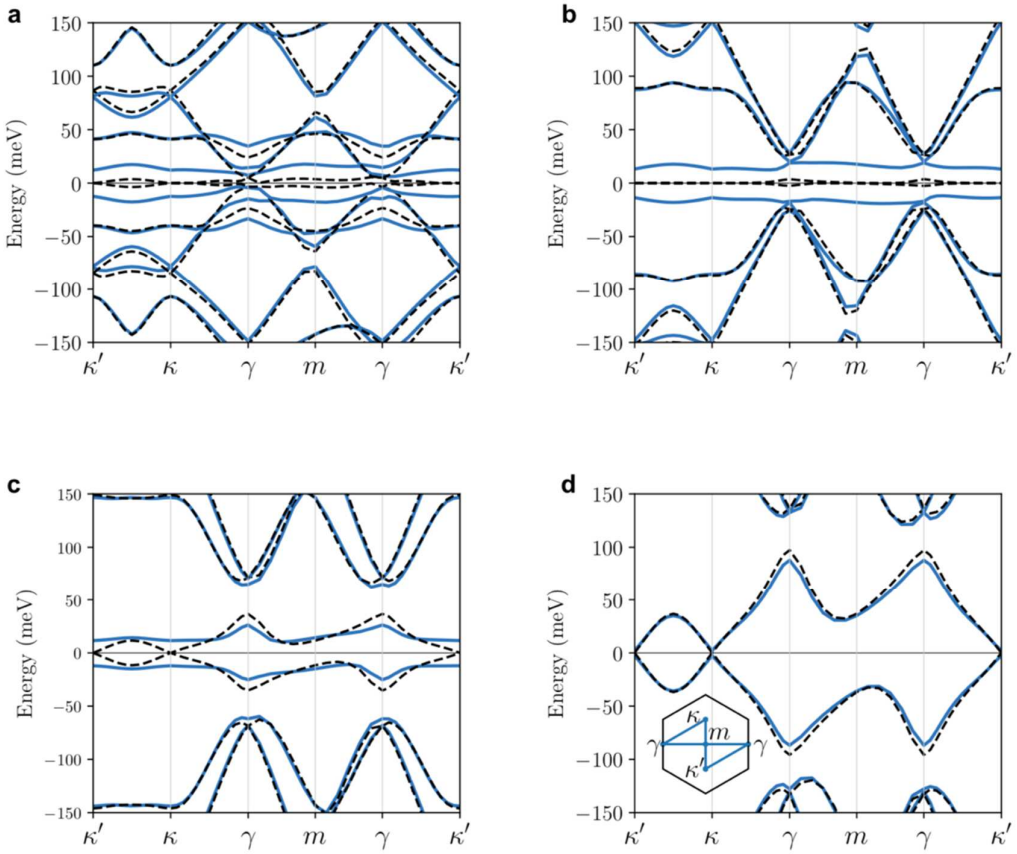

Figure S7| Quasiparticle bandstructures obtained by performing self-consistent mean field ground states at neutrality ($\nu = 0$) with twist angle a, θ=0.85°, **b,** θ=1.10, **c,** θ=1.40° and **d,** θ=1.80°. The interaction strength parameter used for all this calculations was $\varepsilon^{-1} = 0.06$. The dashed lines illustrate the non-interacting bandstructure as comparisons. Case **b** is close to the magic angle condition. The inset of **d** shows the moiré Brillouin zone and its high symmetry points. These plots are results of single flavor calculation, which differs only slightly from four flavor calculations at neutrality.

Fig. S7 shows the mean field quasiparticle bandstructures for different phases across the phase diagram shown Fig. 1g. We fixed the interaction strength to be $\varepsilon^{-1} = 0.06$ as an example. The four twist angles fall into three distinct ground states as classified in Fig 1g. Fig. S7a and Fig.

7b correspond to states that break C_2T symmetry. While the highest valence band of Fig. 14a has a nonzero Chern number, it vanishes for Fig.S7c. Fig. S7b and Fig. S7d correspond to states which do not break C_2T symmetry but still have a finite charge gap. The mechanism of gap opening in this case is unusual and involves the annihilation of the flat band Dirac points by Dirac points sourced by band crossings between flat bands and remote higher energy bands. It is evident in the Fig. S7a and Fig. S7b that the originally isolated flat bands get "pushed" into the higher energy bands by interactions and have band touching points with them away from high symmetry momenta. The difference between non-zero Chern number (Fig. S7a) and zero Chern number (Fig. S7c) bands is related to band touchings with the higher energy bands. We remark that the interaction strength in (Fig. S7c) is weak in comparison to the band gap between flat bands and higher bands. The dominant interaction effects shown in these plots is renormalization of the lowest bands only.

I. Quasiparticle Bandstructure of an Insulating Ground State at $\nu = -1$

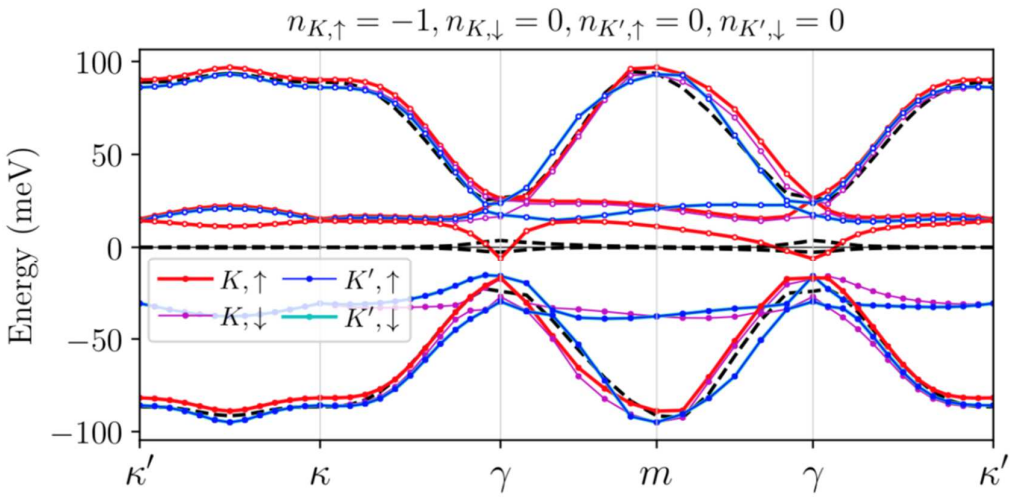

Figure S8 | Four-flavor quasiparticle bandstructures for an insulating ground states at $\nu = -1$ at magic angle θ=1.10°. We chose $\varepsilon^{-1} = 0.06$ as an example. The black dashed lines are the non-interacting bandstructures, which are shown for comparison. Filled and empty circle markers represent occupied and unoccupied bands, respectively. We plot the lowest four bands, i.e. two conduction and two valence bands, for each flavor. $n_{K(K'),\uparrow(\downarrow)}$ is defined in unit of n_0. The ground state spontaneously polarizes to $|K,\uparrow\rangle$ flavor.

Fig. S8 shows the quasiparticle bandstructure for filling factor $\nu = -1$. The ground state spontaneously breaks the SU(4) flavor symmetry by emptying the highest valence band of $|K,\uparrow\rangle$ flavor. This emptied valence band is shifted up and separated from the quasi-degenerate valence bands of the other flavors. Depending on the detailed parameters, the ground state may either be insulating with a small gap or semi-metallic with a small band overlap. For this value of ε^{-1} the ground state is semi-metallic with a small band overlap, which occurs not along the high symmetry lines and is therefore not visible in this plot. The bandstructures at other filling factors can be understood in a similar way

References

1 Bistritzer, R. & MacDonald, A. H. Moiré bands in twisted double-layer graphene. *Proceedings of the National Academy of Sciences* **108**, 12233-12237 (2011).

2 Xie, M. & MacDonald, A. H. On the nature of the correlated insulator states in twisted bilayer graphene. *arXiv preprint arXiv:1812.04213* (2018).

3 Carr, S., Fang, S., Zhu, Z. & Kaxiras, E. Minimal model for low-energy electronic states of twisted bilayer graphene. *arXiv preprint arXiv:1901.03420* (2019).